

**SEISMIC ATTENUATION, EVENT DISCRIMINATION, MAGNITUDE AND
YIELD ESTIMATION, AND CAPABILITY ANALYSIS**

Michael E. Pasyanos, William R. Walter, Eric M. Matzel,
Rengin Gök, Douglas A. Dodge, Sean R. Ford, and Arthur J. Rodgers

Lawrence Livermore National Laboratory

Sponsored by the National Nuclear Security Administration

Award No. DE-AC52-07NA27344/LL09-IRP-NDD02

ABSTRACT

We present the latest results on Lawrence Livermore National Laboratory's calibration efforts for seismic attenuation of regional body and surface waves that have application to many different areas of nuclear explosion monitoring. We have developed methods that use amplitude measurements of the direct regional phases (Pn, Pg, Sn, Lg) to determine the attenuation structure of the lithosphere in Eurasia. The amplitudes are inverted simultaneously for attenuation parameters (Q_p , Q_s) of the crust and upper mantle, along with event source terms and station site terms. We are applying similar methodologies to coda amplitudes. Like direct waves, coda waves are subject to path-dependent variations in amplitudes. We see geographic similarities between the crustal shear-wave attenuation and the results from the coda attenuation. Calibration of coda in the Middle East and other areas is complicated by the fact that the dominant S-wave phase is either Sn or Lg depending on tectonic region, distance, and frequency. Over the past year, we have made great progress on the calibration of surface wave attenuation with the development of the Surface Wave Amplitude Processor (SWAP). With this tool, we are able to make surface wave amplitude measurements quickly, reliably, and consistently. We will be presenting a preliminary surface wave attenuation tomography of the Middle East.

Regional attenuation models are directly applicable to event discrimination, such as high-frequency regional P/S discriminants (e.g., Pn/Lg, Pg/Lg, Pn/Sn) and longer period $M_s:m_b$. Correcting the observed amplitudes for path-dependent variations reduces scatter in the earthquake population and increases separation from explosions. Better body-wave path corrections might even allow the extension of P/S discrimination to lower frequencies so long as true source differences between events exist at those frequencies. Similarly, surface wave attenuation structure can be used to reduce scatter in earthquake surface wave amplitudes and might allow extension of the $M_s:m_b$ discriminants to higher frequency M_s that can be measured on smaller events. Surface-wave models can also provide useful constraints on the attenuation structure of aseismic regions which are not well-sampled by the regional body-wave phase tomography. Coda attenuation calibration methods can be used to improve the coda magnitude estimates that are useful for reliable yield estimation, allowing the method to be applied over broad and complex regions. We can use these attenuation models, along with associated earthquake and explosion source models, to predict expected signal-to-noise at a station for a given combination of phase, frequency, path, magnitude, etc. This is useful for creating magnitude thresholds maps for regional discriminants, and for event detection and location. Such regional attenuation-based threshold maps are needed to understand monitoring capability as event size is lowered and signals are only detectable mainly at local and regional distance ranges.

OBJECTIVES

Our first objective is to develop methods to determine the earth's attenuation structure. Coupled with information on the earth's velocity structure, the models can be used to predict the amplitudes of a variety of seismic phases, including direct regional phases, surface waves, and coda. Our other main objective is to use this information in a variety of methods in order to improve our ability to discriminate events, estimate magnitude and yield, and in providing information on monitoring capability.

RESEARCH ACCOMPLISHED

In the past year, we have accomplished a number of research goals in seismic attenuation (including improved regional attenuation maps and the development of a new surface wave attenuation tool), event discrimination (calibrated high-frequency P/S discriminants, mb:Ms), improved magnitude and yield estimation (derived from path-corrected coda amplitudes), and tools for providing capability assessment.

Seismic Attenuation

LLNL has developed a four-phase amplitude tomography which allows us to determine a set of attenuation, site, and source corrections for the primary regional phases of Pn, Pg, Sn, and Lg. Our basic methodology, employed in Pasyanos et al. (2009a) for Lg, uses an MDAC source model (Walter and Taylor, 2001), which more explicitly defines the source expression in terms of an earthquake source model formulated in terms of the seismic moment. We applied the technique to simultaneously invert amplitudes of Pn, Pg, Sn and Lg in the Middle East to produce P-wave and S-wave attenuation models of the crust and upper mantle for the region (Pasyanos et al., 2009b).

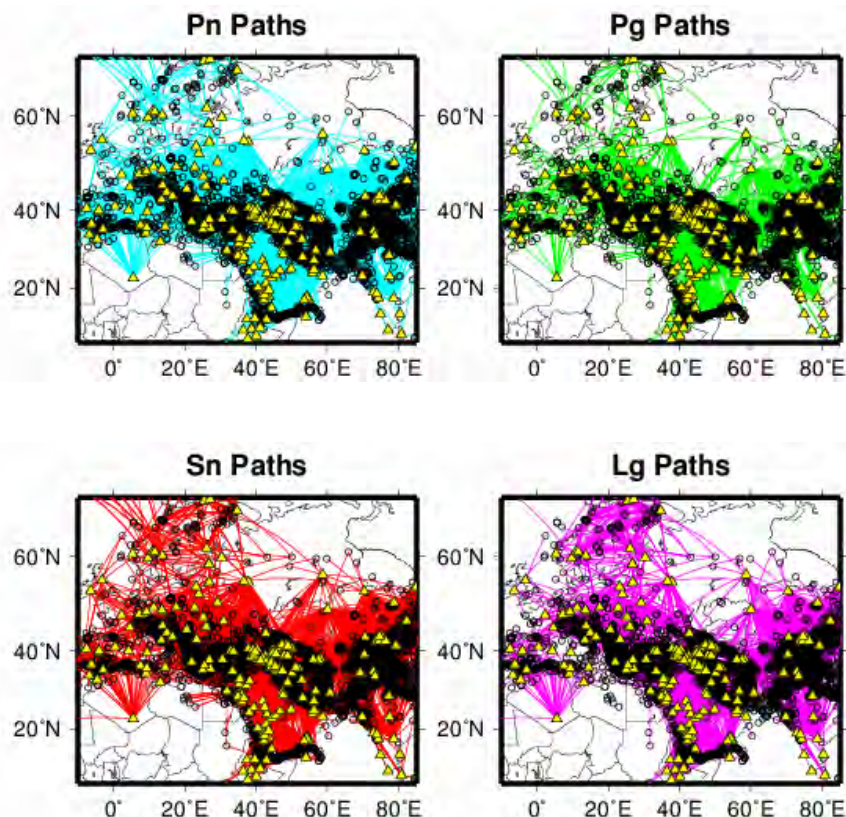


Figure 1. Path map of Pn, Pg, Sn, and Lg attenuation measurements for western and central Eurasia in the 1-2 Hz passband.

Here, we have extended the region into Europe to cover all of western Eurasia and portions of north Africa, as shown by the path maps in Figure 1. The attenuation is modeled as P-wave and S-wave attenuation layers for the

crust, and a similar set for the upper mantle. Inverting all of the phases simultaneously allows us to determine consistent attenuation, site, and source terms for all phases, and eliminates non-physical inconsistencies among them. Preliminary results are shown in Figure 2.

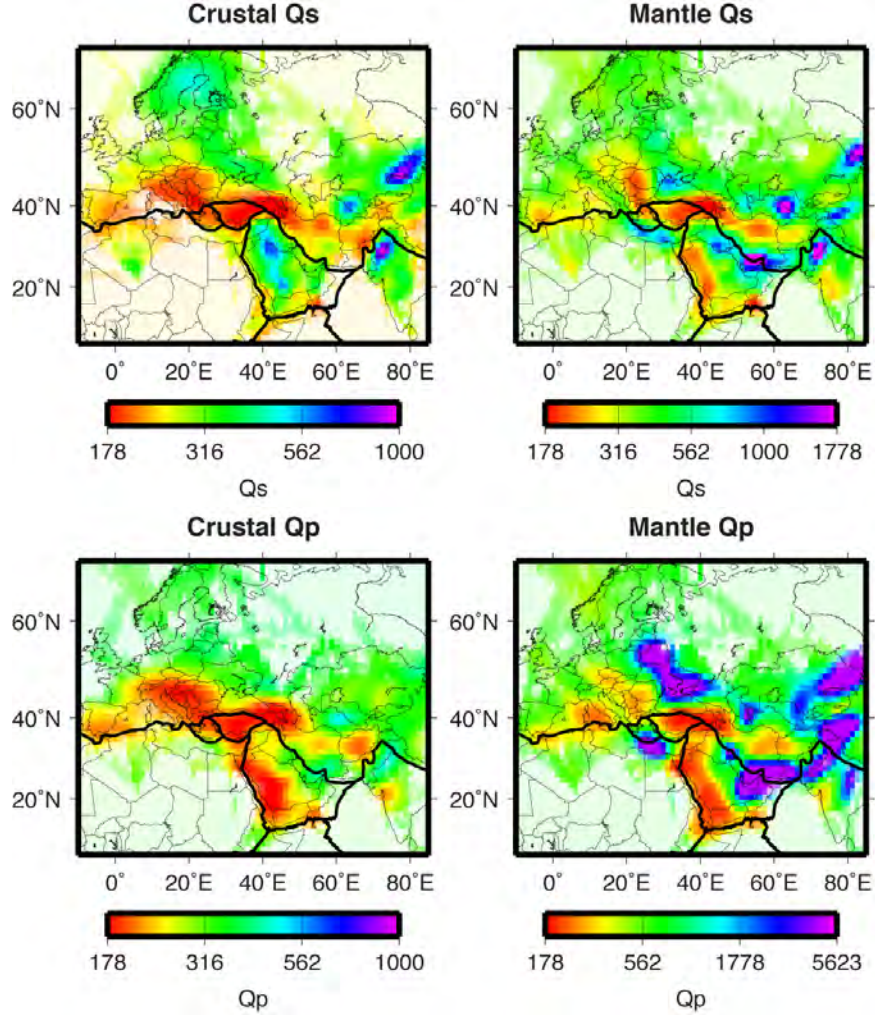


Figure 2. Attenuation of crustal Qs, mantle Qs, crustal Qp, and mantle Qp of western and central Eurasia in the 1-2 Hz passband.

We are applying similar methodologies to coda amplitudes, derived using the coda wave method (Mayeda and Walter, 1996; Mayeda et al., 2003). With this technique, the analytic expression used to fit the observed narrowband envelopes at the center frequency f as a function of distance r (in kilometers) for times greater than the direct S -wave arrival is

$$A_c(f, t, r) = W_o(f) \bullet S(f) \bullet T(f) \bullet P(r, f) \bullet H\left(t - \frac{r}{v(r)}\right) \bullet \left(t - \frac{r}{v(r)}\right)^{-\gamma(r)} \bullet \exp\left[b(r) \bullet \left(t - \frac{r}{v(r)}\right)\right] \quad (1)$$

where $W_o(f)$ is the S -wave source amplitude, $S(f)$ is the site response, $T(f)$ is the S -to-coda transfer function resulting from scattering conversion, $P(r, f)$ includes the effects of geometrical spreading and attenuation (both scattering and absorption), H is the Heaviside step function, t is the time in seconds from the origin, $v(r)$ is the velocity of the peak arrival in km/sec, and $\gamma(r)$ and $b(r)$ control the coda envelope shape.

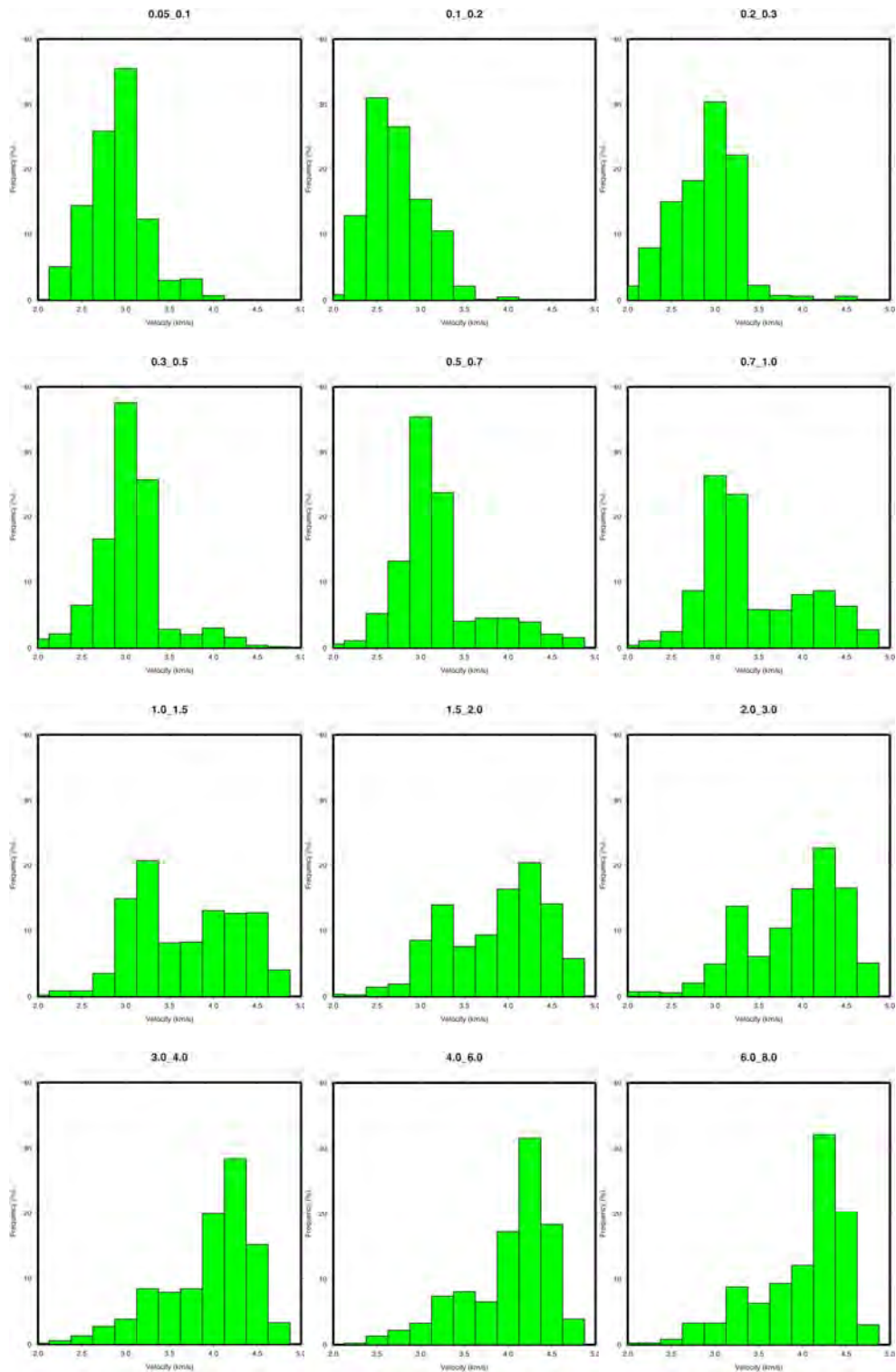


Figure 3. Peak velocities of coda envelopes for paths in the Middle East. Each plot shows a histogram of the velocities in narrow frequency bands: 0.05-0.1, 0.1-0.2, 0.2-0.3, 0.3-0.5, 0.5-0.7, 0.7-1, 1-1.5, 1.5-2.0, 2-3, 3-4, 4-6, and 6-8 Hz.

Like direct waves, coda waves are subject to path dependent variations in amplitudes. We see geographic similarities between the crustal shear-wave attenuation and results from the coda attenuation. Calibration of coda in the Middle East and other areas is complicated by the fact that the dominant S-wave phase varies depending on tectonic region, distance, and frequency. Figure 3 shows the peak velocities of coda paths in the Middle East as a function of frequency. At the lowest frequencies (0.05-0.1 Hz or 10-20 sec, 0.1-0.2 Hz or 5-10 sec), the coda is dominated by surface waves and we see velocities consistent with short period group velocities (2.0-3.0 km/s). At more intermediate frequencies (0.2-0.3 Hz, 0.3-0.5 Hz, 0.5-0.7 Hz, 0.7-1.0 Hz), the velocities are peaked around typical Lg velocities of 3.2 km/s. At higher frequencies (1-1.5 Hz, 1.5-2 Hz, 2-3 Hz), we see the emergence of another peak at faster velocities more typical for Sn propagation (4.0-4.5 km/s). Where one or the other dominates depends on the propagation region. By the highest frequencies (3-4 Hz, 4-6 Hz, 6-8 Hz), we see that these higher-velocity Sn peaks dominate the lower-velocity Lg peaks.

LLNL has recently completed the development of the Surface Wave Amplitude Processor (SWAP) tool, which is intended to aid in the production of high quality amplitude measurements of surface wave amplitudes (Dodge et al., 2010). It utilizes the NNSA moment tensor schema and NASA World Wind software. The user can select stations and events according to a number of criteria (station and event location, magnitude, etc.), and then select the best channel set for measurements (Figure 4). The instrument response is removed and the traces are rotated into radial and transverse orientation, allowing Rayleigh and Love wave measurements. A comb of narrow-band filters allows the user to easily select the band of frequencies over which surface wave measurements are to be performed (Figure 4). Amplitudes are measured in the frequency-domain, time domain RMS, and time domain peak-to-peak, allowing the measurements to be used in a number of applications. The tool also records the source amplitudes as predicted by the moment tensor solution, allowing the ability to discard measurements from radiation nodes, which are contaminated by multi-pathing.

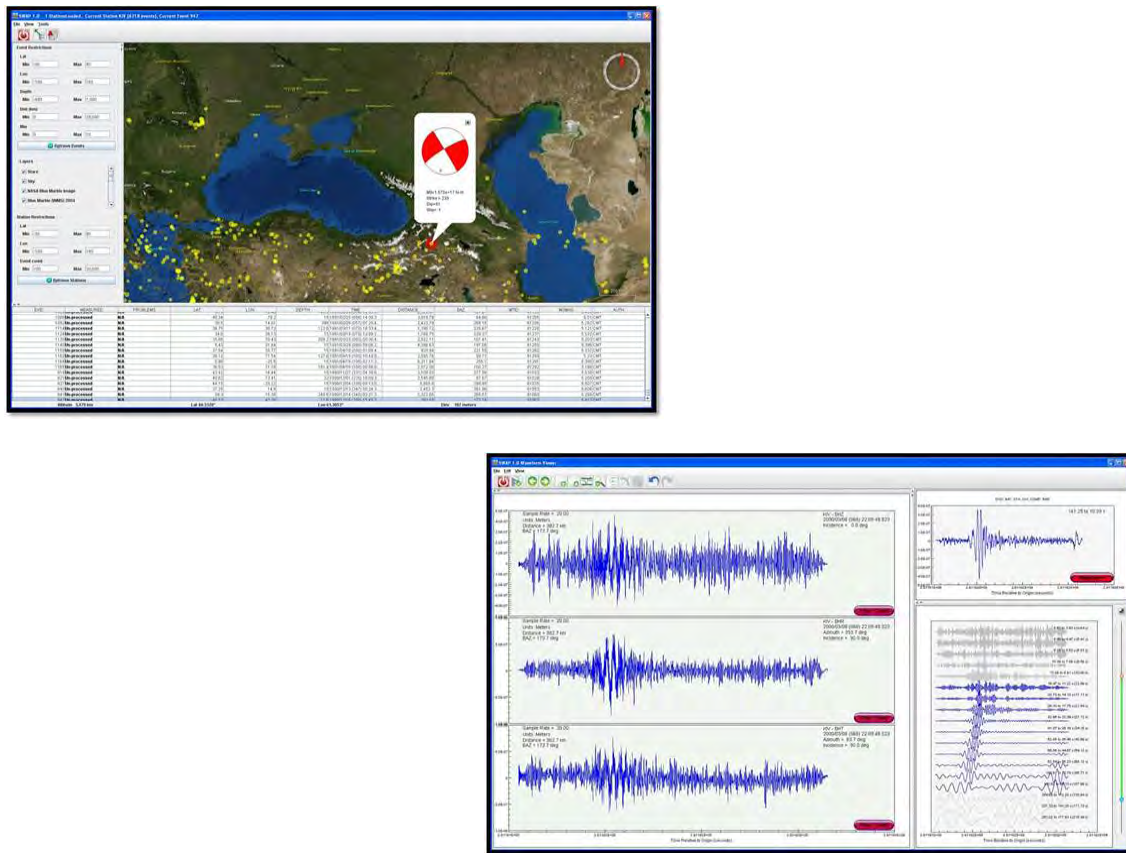


Figure 4. The SWAP Main and Waveform Dialog Boxes.

Event Discrimination

It has been demonstrated that applying corrections with the attenuation models can significantly improve earthquake-explosion discrimination using high-frequency regional P/S amplitude ratios (Pasyanos and Walter, 2009). P/S discriminants are expressed as the ratio between the P-wave amplitude (A^P) and the S-wave amplitude (A^S) and, because of the large variations, are usually plotted on a log scale. To correct the phase ratio for path and source effects, we adjust the individual amplitudes assuming an earthquake source. We then form our discriminant using the ratio of the corrected amplitudes:

$$\text{discriminant} = \log \left[\frac{(A^P / A_0^P)}{(A^S / A_0^S)} \right] = \log \left[\frac{A^P}{A^S} \right] - \log \left[\frac{A_0^P}{A_0^S} \right] \quad (2)$$

where A_0 are the amplitude predictions for an earthquake of that phase and size. As a result, the corrected discriminant should now have a value around 0 (P/S ratio of 1) for earthquakes. We input a best estimate of the earthquake size by using a moment magnitude, if available, or otherwise estimating M_w using other magnitude estimates. Using the extended attenuation results, we intend to show discrimination examples beyond our previous work for the India and DPRK nuclear explosions.

A well-known and widely-used discriminant is a comparison of the body-wave and surface-wave magnitudes of an event, or mb:Ms. In recent years, the Ms(VMAX) formula (Russell, 2006) has been widely used in the explosion monitoring community. Because it uses periods between 8 and 25 sec, rather than at the traditional 20 sec, the method can effectively measure surface wave magnitudes at both regional and teleseismic distances. The formula is given below:

$$M_{s(b)} = \log(a) + \frac{1}{2} \log(\sin(\Delta)) + 0.0031 \left(\frac{20}{T} \right)^{1.8} \Delta - 0.66 \log \left(\frac{20}{T} \right) - \log(f_c) - 0.43 \quad (3)$$

where a is the amplitude, D the distance, T the period, and f_c the corner filter frequency. Built into this formula is a 1-D attenuation structure, which will obviously not be valid for many paths, especially at the more highly-variable shorter periods. The surface wave attenuation structure can be used to reduce scatter in earthquake surface wave amplitudes. For example, the third term in equation (3) would be replaced by a path-specific attenuation term. We are still researching how much of an effect correcting M_s for attenuation would have on $M_s(\text{VMAX})$ and the mb:Ms discriminant.

Magnitude and Yield Estimation

Coda attenuation calibration methods can be used to improve the coda magnitude estimates that are useful for reliable yield estimation, allowing the method to be applied over broad and complex regions. Figure 5 compares paths from an event in the Strait of Hormuz recorded at ten regional stations. The panel on the bottom left shows moment rate functions that have been corrected with a 1-D path correction without site terms. In comparison, the panel on the bottom right shows the moment rates for the same paths, where the amplitudes have had a 2-D path correction applied. The combination of site terms and path specific attenuation results in a much more consistent estimation of the earthquake source.

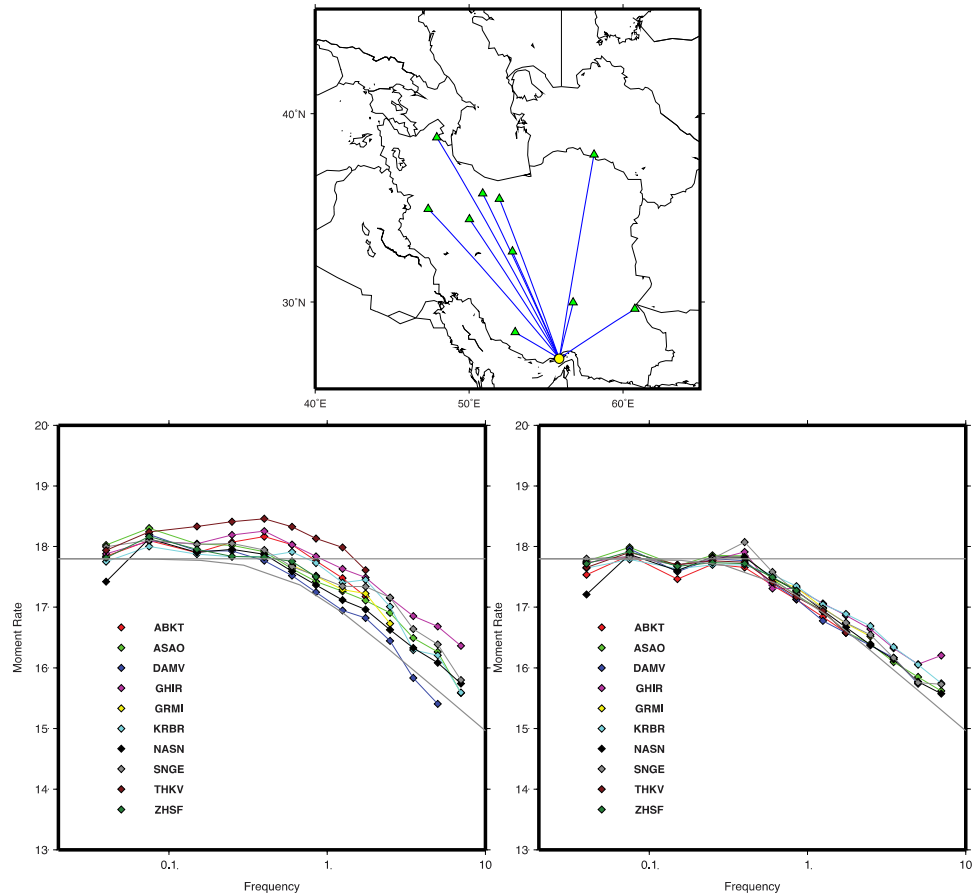


Figure 5. An event in the Strait of Hormuz recorded at ten regional stations. The bottom figures show the comparison of the moment rate functions with 1-D and 2-D path corrections.

Analysis

We can use our regional attenuation models, along with associated earthquake and explosion source models, to predict expected signal-to-noise at a station for a given combination of phase, frequency, path, magnitude, etc. Figure 6 shows an example of maps with predicted signal-to-noise of an Mw 4.0 earthquake recorded at station UOSS in Sharjah, UAE using an average noise level for the station. The panel to the left shows SNR for Sn in the 2-4 Hz passband, while the panel to the right shows 2-4 Hz Lg. Plotted on top are observed signal-to-noise from events with magnitudes around 4.0. There is some variation in the observations due to changes in the background noise level and the individual event magnitudes sometimes being slightly higher or lower than magnitude 4.0. Figure 7 shows the progression of the capability maps at the same station for Sn in the 2-4 Hz, 4-6 Hz, and 6-8 Hz passbands. Lastly, Figure 8 shows a similar progression where event size progresses from Mw 5.0 to Mw 4.0 and down to Mw 3.0. Using Mueller-Murphy (Mueller and Murphy, 1971), we can make similar figures for explosions of a given yield, depth, and shot material.

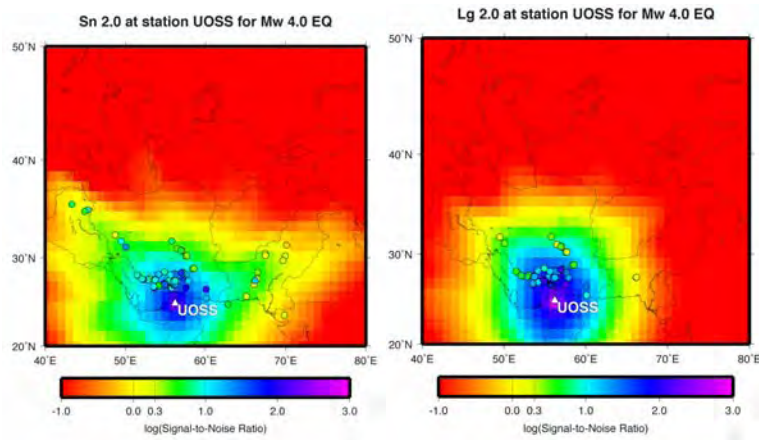


Figure 6. Expected signal-to-noise of an Mw 4.0 earthquake recorded at station UOSS in Sharjah, UAE for 2-4 Hz Sn and Lg. Colored symbols show observed SNR from events.

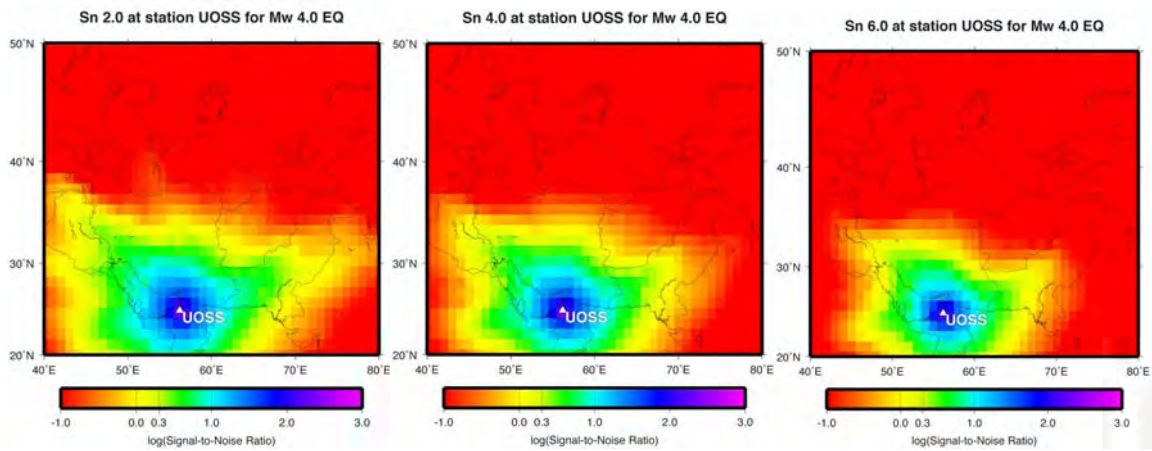


Figure 7. Expected signal-to-noise of an Mw 4.0 earthquake recorded at station UOSS for Sn in 2-4 Hz, 4-6 Hz, and 6-8 Hz.

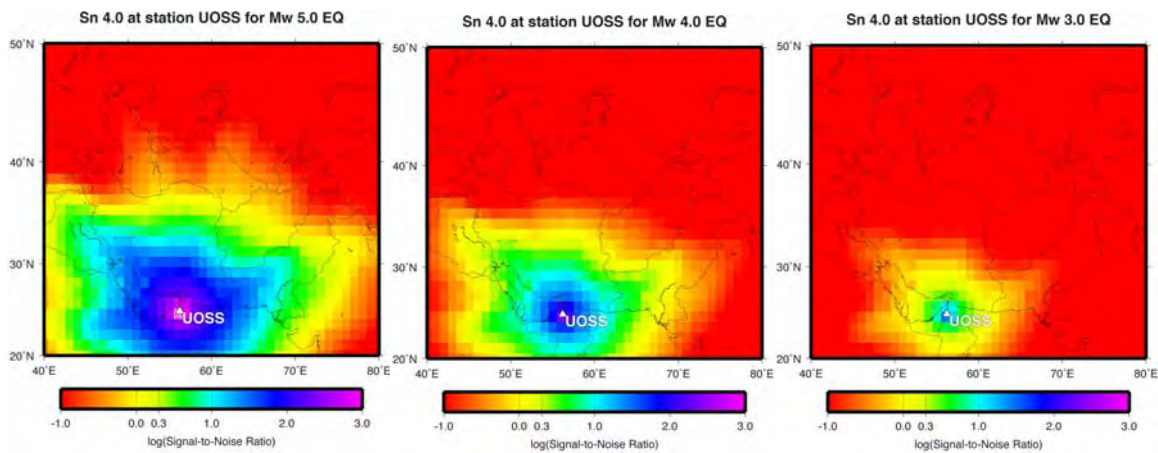


Figure 8. Expected signal-to-noise of 4-6 Hz Sn recorded at station UOSS or Mw 5.0, Mw 4.0, and Mw 3.0 events.

CONCLUSIONS AND RECOMMENDATIONS

The calibration of the earth's attenuation structure, coupled with calibration of velocity structure, allows us to predict the amplitudes of a variety of seismic phases. This predictive capability allows us to improve our event identification, as has been demonstrated with the high-frequency regional P/S discriminant, and as we intend to demonstrate with mb:Ms. Our model also allows us to make improved magnitude and yield estimates, and can be used in station and network capability analysis. It is recommended that the attenuation calibrations be tested for use in nuclear explosion monitoring operations.

ACKNOWLEDGMENTS

We thank Stan Ruppert and Terri Hauk for maintaining the LLNL Seismic Research Database. We thank Mike Ganzberger and Kathy Dyer for their contributions to the RBAP and SWAP codes, used to make regional and surface wave amplitude measurements. We thank Gene Ichinose for the regional moment magnitudes used in the coda calibration.

REFERENCES

- Dodge, D. A., M. D. Ganzberger, T. F. Hauk, and S. D. Ruppert (2010). Enhancing seismic calibration research through software automation and scientific information management, in *Proceedings of the 2010 Monitoring Research Review: Ground-Based Nuclear Explosion Monitoring Technologies*, LA-UR-10-05578, Vol. 2, pp.743–752.
- Mayeda, K., A. Hofstetter, J. L. O'Boyle, W. R. Walter (2003). Stable and transportable regional magnitudes based on coda-derived moment-rate spectra. *Bull. Seismol. Soc. Am.* 93: 224–239.
- Mayeda, K. and W. R. Walter (1996). Moment, energy, stress drop, and source spectra of western U.S. earthquakes, *J. Geophys. Res.* 101: 11195–11208.
- Mueller R. A. and J. R. Murphy (1971), Seismic characteristics of underground nuclear detonations: Part I. seismic spectrum scaling, *Bull. Seismol. Soc. Am.* 61: 1675–1692.
- Pasyanos, M. E. and W. R. Walter (2009). Improvements to regional explosion identification using attenuation models of the lithosphere, *Geophys. Res. Lett.*, doi:10.1029/2009GL038505.
- Pasyanos, M. E., E. M. Matzel, W. R. Walter, and A. J. Rodgers (2009a). Broad-band Lg attenuation modeling of the Middle East, *Geophys. J. Int.*, 177: 1166–1176, doi:10.1111/j.1365-246X.2009.04128.x
- Pasyanos, M. E., W. R. Walter, and E. M. Matzel (2009b). A simultaneous multi-phase approach to determine P-wave and S-wave attenuation of the crust and upper mantle, *Bull. Seism. Soc. Amer.*, 99-6., 3314–3325, doi:10.1785/0120090061.
- Russell, D. R. (2006). Development of a time-domain, variable-period surface wave magnitude measurement procedure for application at regional and teleseismic distances, Part I: Theory, *Bull. Seismol. Soc. Am.*, 96: 665–677.
- Walter, W. R. and S. R. Taylor (2001). A revised magnitude and distance amplitude correction (MDAC2) procedure for regional seismic discriminants: theory and testing at NTS, Lawrence Livermore National Laboratory, UCRL-ID-146882, <http://www.llnl.gov/tid/lof/documents/pdf/240563.pdf>